ADVANCED MATERIALS
www.advmat.de

www.MaterialsViews.com

A Self-Powered, Sub-nanosecond-Response Solution-Processed Hybrid Perovskite Photodetector for Time-Resolved Photoluminescence-Lifetime Detection

*Liang Shen, Yanjun Fang, Dong Wang, Yang Bai, Yehao Deng, Mengmeng Wang, Yongfeng Lu, and Jinsong Huang**

Ultrafast solid-state semiconductor photodetectors have many important applications, including fast imaging, high-speed optical communication, and monitoring of ultrafast dynamic processes, in the fields of consumer electronics, industry, defense, and academic research.[1,2] These devices heavily rely on traditional inorganic semiconductor materials, such as silicon, indium gallium arsenide, gallium nitride,[3–5] which are generally deposited by expensive, slow, high-temperature processes, such as molecular-beam epitaxy and metal–organic chemical vapor deposition. Solution-processed semiconductors, including organic semiconductors and nanomaterials, are increasingly exploited in photodetection applications due to their many intrinsic advantages. These materials can be deposited by established, low-cost, versatile solution techniques, such as spin coating, slot-die coating, inkjet printing, and gravure coating,[6–9] on many different types of substrates, both rigid and flexible, and even on curved surfaces.[10] Large-size arrays can be directly printed with high-throughput printing processes, which avoid the patterning steps in traditional semiconductor techniques. There has been tremendous progress made during the past decade on improving the sensitivity, extending the response spectrum to ultraviolet and near infrared, and increasing the linear dynamic range of these solution-processed photodetectors.[11–13] Today, the sensitivity of solution-processed photodetectors has already surpassed that of traditional inorganic semiconductor photodetectors in most spectral ranges, including the ultraviolet, visible, and near-infrared; and the linear dynamic range has also surpassed that of the best inorganic photodetectors.[14,15] Nevertheless, despite the significant progress on the aforementioned aspects, one grand challenge still to be addressed is the low response speed of solution-processed photodetectors. For solution-processed photodetectors to be used as imagers in consumer electronics, millions of pixels need to be read out in a short time (milliseconds or less) for each image frame; and the frame rate needs to be high enough to display consecutive images. Most organic semiconductors have low drift mobility, <0.01 $cm^2\ V^{-1}\ s^{-1}$,[16] making the response speed of organic photodetectors generally in the megahertz range, despite the small active-layer thickness of <200 nm.[17] Photodetectors made of inorganic semiconductor nanoparticles generally employ lateral structures due to the difficulty of forming leakage-free, compact films for vertical structure devices; therefore, the charge transit time is much longer than in vertical-structure devices due to the long channel length, despite their larger mobility, in the range of 0.1–30 $cm^2\ V^{-1}\ s^{-1}$.[18] In addition, the presence of charge traps in many of these solution-processed semiconductors is sometimes intentionally introduced to generate a photoconductive gain,[14,19,20] inevitably slowing down their response speed.

Organic–inorganic hybrid perovskites (OIHP) have recently emerged as a new generation of promising materials for solar cell absorbers, yielding power conversion efficiencies of >20% within only five years of development, benefiting from their outstanding intrinsic optoelectronic properties, including tunable bandgap, high absorption coefficient, low exciton-binding energy, high mobility, and long carrier diffusion length.[21–23] Recently, the application of OIHP was widely broadened to other fields, such as light-emitting diodes, lasers, photodetectors, X-ray detectors, and so on.[24–28] For OIHP photodetectors, both the high-gain photoconductive type and the low-noise photodiode type, have been recently reported.[29–31] OIHP photodetectors also have a unique advantage in their use as the imager in digital cameras because their proper bandgap enables a response only to visible light, while silicon-based imagers always need a filter to block infrared light and enhance the imaging quality. Despite rapid progress in the sensitivity enhancement of perovskite photodetectors, little is known about how fast the OIHP photodetectors can operate.

Herein, we report a solution-processed photodetector based on OIHP with a sub-nanosecond response time at zero-bias operation. The high mobility of a perovskite absorber layer and ultralow trap density as a result of charge-trap passivation enable efficient, fast charge-carrier extraction. The fast response and power-free operation provide an opportunity to measure the charge-carrier radiative recombination lifetime by monitoring photoluminescence decay, which is one typical application of ultrafast photodetectors. A time-resolved photoluminescence (TRPL) system has been demonstrated with the OIHP photodetectors, a pulse laser, and an oscilloscope which has successfully resolved the photoluminescence lifetime of several typical

Dr. L. Shen, Dr. Y. Fang, D. Wang, Dr. Y. Bai, Y. Deng, Prof. J. Huang
Department of Mechanical and Materials Engineering
University of Nebraska-Lincoln
Lincoln, NE 68588-0656, USA
E-mail: jhuang2@unl.edu
Dr. M. Wang, Prof. Y. Lu
Department of Electrical and Computer Engineering
University of Nebraska-Lincoln
Lincoln, NE 68588-0656, USA

DOI: 10.1002/adma.201603573

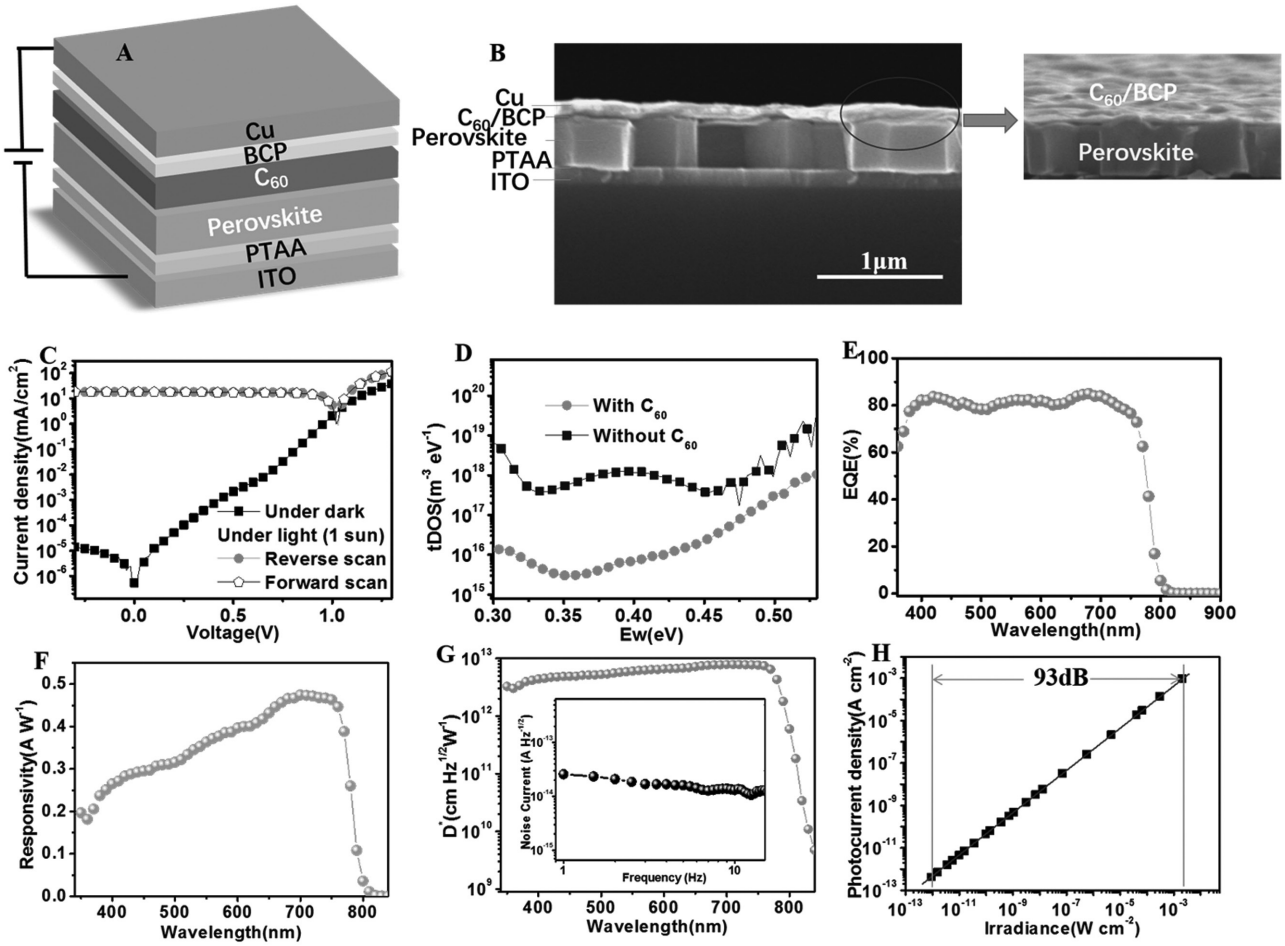

Figure 1. Device structure and photodetection performance under steady light. A) Schematic device structure of the OIHP photodetectors. B) Cross-section SEM image of an OIHP photodetector. Inset: a tilted view of perovskite and C_{60}/BCP layer. C) Current-density–voltage (*J*–*V*) characteristics: photocurrent density at 100 mW cm^{-2} by reverse and forward scanning, and dark-current density of the OIHP photodetectors. D) The trap density of states curve versus demarcation energy with or without C_{60} in the devices. E) EQE of the OIHP photodetector at zero bias. F) Responsivity of the OIHP photodetector at –0.1 V. G) The specific detectivity of the OIHP photodetector at different light wavelengths under –0.1 bias. Inset: The noise current of the OIHP photodetector at –0.1 V. H) The linear dynamic range of the OIHP photodetector under an LED illumination of various light intensities. The solid line represents linear fitting to the data.

fluorescent and phosphorescent materials without resorting to an ultrafast preamplifier.

The device structure of the OIHP photodetectors developed in this study is displayed in **Figure 1**A. It is similar to our previously reported perovskite solar cells, but the electron extraction layer was changed to fullerene (C_{60}) only instead of a phenyl-C61-butyric acid methyl ester ($PC_{61}BM$)/C_{60} double layer to enhance its response speed because the mobility of C_{60} is at least one order of magnitude higher than that of $PC_{61}BM$.[32] The structure was composed of indium tin oxide (ITO)/poly(bis(4-phenyl)(2,4,6-trimethylphenyl)amine (PTAA)/$CH_3NH_3PbI_3$ ($MAPbI_3$)/C_{60}/2,9-dimethyl-4,7-diphenyl-1,10-phenanthroline (BCP)/copper (Cu). In the device structure, each layer was carefully selected. The nonwetting PTAA played an important role in increasing the grain size and decreasing the grain boundary area,[33] which can clearly be seen in Figure 1B from the cross-section of a scanning electron microscopy (SEM) image of the perovskite film on PTAA. Each perovskite grain was directly connected to a cathode and an anode, which indicates that the 500 nm thin film's perovskite layers can be regarded as many single crystals for charge transport and collection. It can also be seen that the 30 nm C_{60}/8 nm BCP can completely cover the perovskite layer, avoiding direct contact between the perovskite layer and cathode metal to avoid a possible reaction between them. Figure 1C displays the dark current and photocurrent density curve (under air mass 1.5 global illumination) of the OIHP photodetectors under forward and reverse scanning between –0.3 and 1.6 V. The dark current density was 1.4×10^{-5} mA cm^{-2} under –0.3 V, which was low enough to resolve light as weak as a sub-picowatt per square centimeter, as demonstrated in our previous report.[31] This low dark current can be attributed to the fact that the C_{60} layer completely covered the perovskite layer and effectively reduced the current leakage. Figure 1D displays the measured trap density of state (tDOS) using the thermal admittance spectroscopy method before and after introducing C_{60}. There was a relatively large density of defect state of 1×10^{17}–1×10^{19} m^{-3} eV^{-1} in the device without C_{60}. However, the tDOS decreased by nearly two

orders of magnitude for a trap depth below 0.45 eV and by at least one order of magnitude for a trap depth above 0.45 eV. The obvious reduction of tDOS provides direct evidence that C_{60} can effectively reduce perovskite surface traps by passivation, which is important to achieve the fast electron extraction and fast photodetector response reported here. Meanwhile, no photocurrent hysteresis appeared in the photodetectors, which benefited from the passivation role that C_{60} plays in reducing perovskite surface trap density.[34]

Figure 1E shows the wavelength-dependent external quantum efficiency (EQE) measured at 35 Hz and zero bias. The EQE curve is almost flat and above 80% in the whole visible wavelength region, suggesting constant charge-collection efficiency for charges generated by short or long wavelengths near the PTAA surface, as well as in the perovskite grains. The following responsivity curve is shown in Figure 1F, indicating a maximum value of 0.47 A W^{-1} around 680 nm. In order to accurately obtain the noise current of OIHP photodetectors, a fast Fourier transform (FFT) signal analyzer combined with a current preamplifier were used to directly record the noise current at different frequencies. As shown in the inset of Figure 1G, the noise current is as low as 18 pA $Hz^{-1/2}$ and is barely sensitive to the frequency, indicating the successful passivation of the charge traps. Based on the directly measured noise current and R, the specific detectivity (D^*) was calculated[20] and shown in Figure 1G. The specific D^* is above 1.5×10^{12} cm $Hz^{1/2}$ W^{-1} from 350 to 790 nm, with the peak value of 7.8×10^{12} cm $Hz^{1/2}$ W^{-1} at 700 nm. This value is comparable to the commercial Si photodiode at the same wavelength, demonstrating its potential application in the detection of weak visible light. The linear dynamic range of photodetector was measured and is shown in Figure 1H. It can be seen that the responsivity kept almost under light intensity from 0.9 pW cm^{-2} to 2 mW cm^{-2}.

The low trap density and high mobility of the single-crystal-like perovskite layer provided the potential for $MAPbI_3$-based photodetectors to have a fast response. However, the resistance–capacitance (RC) constant of the devices is usually inevitably mixed with carrier transit time, making it difficult to determine the device's response speed limit. The temporal response of a photodetector is characterized by a 3 dB bandwidth, which is the frequency of light signal at which the photoresponse is half of that under steady light. The response bandwidth is affected by both the charge-carrier transit time (t) and the RC constant, and is limited by the slower of the two:[35]

$$f_{-3\mathrm{dB}}^{-2} = \left(\frac{3.5}{2\pi t}\right)^{-2} + \left(\frac{1}{2\pi RC}\right)^{-2} \quad (1)$$

where R is the total series resistance, including the photodiode resistance, contact resistances, and load resistances in the measurement circuit; and C is the sum of the capacitance of the device as well as the parasitic capacitance of the measurement system. To eliminate the RC time-constant influence, the photodetectors, with a varied device area, were investigated first. In this work, the response speed was measured by the transient photocurrent (TPC) method. A short pulse of light from a pulse laser was used to generate carriers in photodetectors which were driven toward the respective electrode by the built-in potential field or an external voltage bias. The induced photocurrent pulse (or TPC curve) was recorded by a fast oscilloscope with an input resistor of 50 Ω. By a single exponential fitting, the response speed can be defined from the linear regime extending out beyond the peak, all the way down to approximately "$1/e$" time of the photocurrent decay. Here, the laser pulse was provided by either a Ti–sapphire femtosecond laser with an emission wavelength of 400 nm, by doubling the frequency and pulse duration of 150 fs at a repeating frequency of 1 kHz, or a nitrogen nanosecond pulse laser with an emission wavelength of 337 nm and pulse duration of 3.5 ns at a repeating frequency of 20 Hz. The response curve was measured by a 1 GHz oscilloscope which had a sampling rate of 5 GHz. It can be seen that the device response times were clearly device-area-dependent: 115.1 ns for 7 mm^2, 35.3 ns for 2 mm^2, 17.9 ns for 1 mm^2, 9.0 ns for 0.5 mm^2, 2.7 ns for 0.15 mm^2, and 0.95 ns for 0.04 mm^2. The response time of 0.95 ns was the fastest response speed reported for OIHP photodetectors, which is at least two orders of magnitude faster than the previous report.[27,30,31,36]

To determine whether we had reached the intrinsic response speed limit of these photodetectors, we did a simple estimation of the transit time of the devices based on the reported carrier mobility of the materials. The detailed calculation can be found in Note 1 in the Supporting Information, which gives a transit time between 0.97 and 3.67 ns, depending on the mobility of C_{60} used, which is dominated by the transit time of the C_{60} layer. It is thus concluded that the measured sub-nanosecond response time was the true device transit time because the RC constant was much shorter than the transit time when the device area was less than 0.04 mm^2 (see Note 2 and Table S1 in the Supporting Information). The rising time of the TPC curve was also limited by the RC constant of the device or the transit time, which was comparable to the decay time for the smallest area devices reported here, regardless of whether the laser pulse durations were 150 fs or 3.5 ns.

We continued to study what limits the measured transit time by examining both the devices and the equipment setup. The devices had three layers: the hole-transport layer, the perovskite layer, and the electron-transport layer, each of which could limit the transit time. We first excluded the PTAA hole-transport layer as the limiting one because of its very small thickness of 1–5 nm and reasonably good hole mobility of 10^{-3} cm^2 V^{-1} s^{-1}. Then we increased the thickness of the perovskite layer from 900 nm to 1.2 μm to find its influence on the transit time measured. As shown in **Figure 2**B, the two TPC curves almost overlapped, with the same response time of ≈1.0 ns. This indicates that the perovskite layer did not limit the transit time despite having the largest thickness in the device structure, which can be explained by its high mobility.[37] Then, we increased the thickness of C_{60} from 30 to 50 and 80 nm. As illustrated in Figure 2C, the response time increased to 1.4 and 2.5 ns for the devices with 50 and 80 nm C_{60}, respectively. The measured transit time constants agreed well with the calculated values with a mobility of 0.05 cm^2 V^{-1} s^{-1} for C_{60} (see Note 1 in the Supporting Information). This clearly shows that the low mobility of C_{60} limited the device response speed when it was too thick. The temperature-dependent device response speed study also confirmed the limiting factor to be the

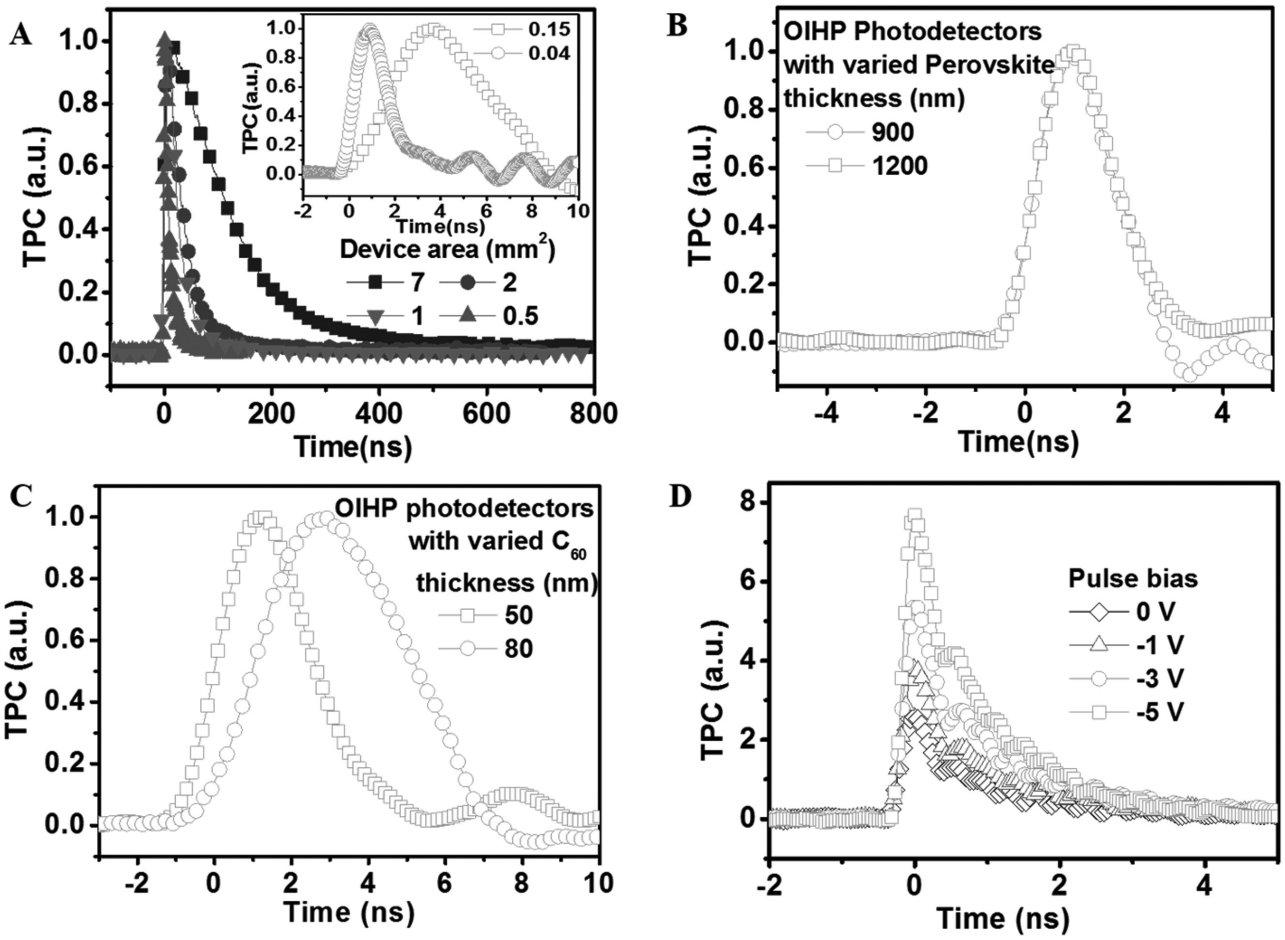

Figure 2. Transient photocurrent measurements of OIHP photodetectors. A) TPC curves of the devices with different areas from 7 down to 0.04 mm^2. TPC lifetime:115.1 ns for 7 mm^2; 35.3 ns for 2 mm^2; 17.9 ns for 1 mm^2; and 9.0 ns for 0.5 mm^2. Inset: 2.7 ns for 0.15 mm^2; 1.0 ns for 0.04 mm^2. B) TPC curves of the perovskite photodetectors with different perovskite thicknesses. C) TPC curves of the perovskite photodetectors with different C_{60} thicknesses. TPC lifetime: 1.4 ns for 50 nm and 2.5 ns for 80 nm. D) Bias-dependent device TPC curves.

fullerene layer (Figure S1, Supporting Information). The device response speed became slower with the reduced temperature. Perovskites have a band-transport property and thus a higher mobility at lower temperatures, while fullerenes have reduced mobility at lower temperatures because of the nature of a thermally activated hopping transport.[38,39] The slowing down of the device response speed originated from the smaller mobility of fullerene at a lower temperature, providing direct evidence that the fullerene layer is the limiting factor at both room temperature and low temperatures. Finally, to further determine whether the response speed is limited by the instrument for the quickest devices with 30 nm C_{60}, a voltage pulse from a Keithley instrument 4200 was applied on the OIHP photodetectors to find their variations in response speed. An increased bias was expected to shorten the transit time by increasing the carrier drift velocity. The pulse bias was applied onto the OIHP photodetectors right before and after a laser pulse to minimize the influence of ion migration so that a large bias could be applied. As shown in Figure 2D, the magnitude of the current increased linearly, while the response time remained invariable at ≈1.0 ns with the applied bias. This indicated that the ≈1.0 ns response time readout from the oscilloscope was limited by the 1 GHz oscilloscope used; and the actual response time was shorter, which agreed with the calculated response time of 0.65 ns for the devices with an active area of 0.04 mm^2 (Table S1, Supporting Information).

It is noted that the response speed of the perovskite photodetectors increased under weaker light excitation, as shown in **Figure 3**A. This can be explained by the decreased screening of the built-in electric field by the photogenerated space-charges.[40] The built-in potential in these photodetectors can be estimated from the *C–V* measurement, which was around 1.1 V (Figure S2, Supporting Information). The energy diagrams of the perovskite photodetector in the dark and under illumination are shown in **Figure 4**B. In the dark, the perovskite layer was completely depleted because the depletion depth derived from the *C–V* measurement covered the whole perovskite thickness (see Note 3 in the Supporting Information). The near intrinsic nature of the perovskite films, as evidenced by results of the Hall effect and ultraviolet photoelectron spectroscopy measurements,[37,41] gave rise to the large depletion width in these devices. Under light, the photovoltage generated by the Fermi level splitting in the perovskite layer was opposite to the built-in potential direction; and the built-in potential was

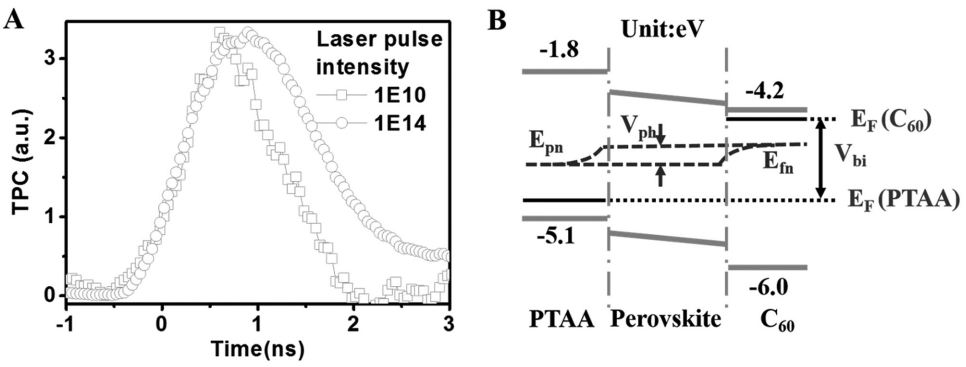

Figure 3. Device response speed at different laser pulse intensities. A) TPC curves of the OIHP photodetector under different laser pulse intensities. B) Schematic layout of V_{bi} variation of the OIHP photodetector under illumination.

thus weakened by the screening effect of the photogenerated charges, resulting in a slower response under stronger excitation for the photodetectors.

We applied the perovskite photodetectors in a TRPL system where an ultrafast photodetector was needed to record the decay process of photoluminescence (PL). The PL lifetime is one of the most important parameters for understanding the properties of optoelectronic materials for applications such as light-emitting diodes, semiconductor lasers, and solar cells.[42–44] It is a critical parameter, reflecting the nature and quality of materials which highly depend on the impurities, defects (both bulk and surface), and presence of dopants.[45] TRPL by time-correlated single photon counting (TCSPC) is generally a method of determining fast charge-carrier dynamics in optoelectronic materials. The essential components of a TCSPC system for measuring PL lifetime include a pulsed laser, single-photon-sensitive photodetector, and optical filters or monochromators to separate the fluorescence signal from excitation

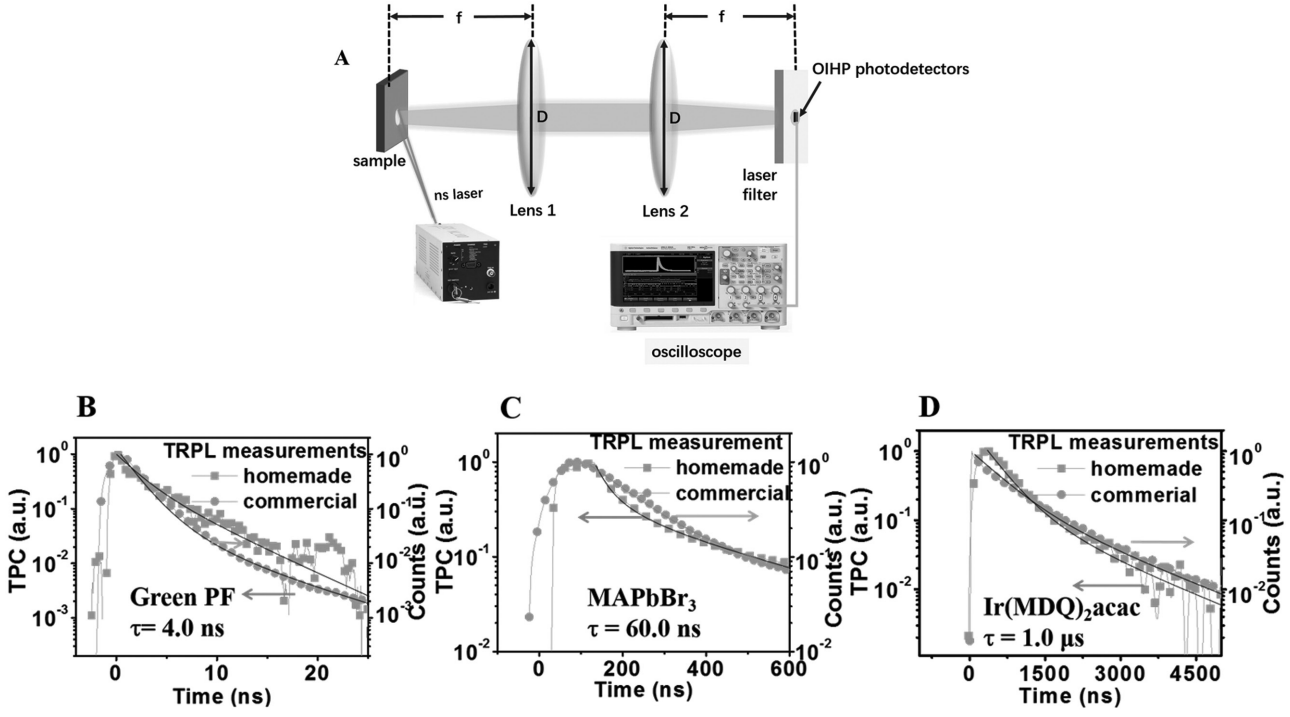

Figure 4. Setup of time-resolved photoluminescence lifetime detection system with OIHP photodetectors. A) Schematic layout of the TRPL system. The nitrogen nanosecond laser acts as an excitation source, which illuminates the sample from a small angle. The sample is located at the focus position of Lens 1 and the photoluminescence from the sample is collected and redirected to a perovskite photodetector by Lens 2. A filter was added to filter the laser scattering emission. A 1 GHz oscilloscope with 50 Ω input resistance was used to connect the perovskite photodetector to record the transient photocurrent curves. B–D) PL decay curves measured by both homemade and commercial systems for green PF (4.0 ns) (B); $MAPbBr_3$ single crystal (60.0 ns) (C); and $Ir(MDQ)_2acac$ (1.0 μs) (D). The solid line represents the exponential fitting to the data.

light and wavelength selection. Our high-sensitivity, sub-nanosecond photodetector provides a good opportunity to monitor the carrier lifetime, because the 1 ns response time was fast enough to follow the lifetime of many conventional semiconductor materials applied for optoelectronic devices. As shown in Figure 4A, a system for measuring carrier lifetime was set up. A nitrogen nanosecond laser was used for excitation. It illuminated the samples from a small angle. The samples were placed at the focus position of Lens 1, and the photoluminescence light from the samples was collected and redirected to a perovskite photodetector by Lens 2. A filter was placed in front of the photodetector to filter the laser scattering emission. The perovskite photodetector was connected to a 1 GHz oscilloscope with 50 Ω input resistance. The signals were recorded in the form of the transient current, and fitting the time decay gave the carrier lifetime. Three types of typical organic and hybrid materials, green polyfluorene (PF), methylammounium lead tri-bromide ($MAPbBr_3$) single crystals, and bis(2-methyldibenzo[f,h]quinoxaline) (acetylacetonate) iridium(III) ($Ir(MDQ)_2(acac)$) were chosen to measure the PL lifetime by the homemade system. The TPC response is shown in Figure 4B–D. By fitting the decay curves, the following lifetimes were derived: ≈4.0 ns for green PF, ≈60.0 ns for the $MAPbBr_3$ single crystals, and ≈1.0 μs for $Ir(MDQ)_2acac$. In order to check the accuracy of these measurements, we also measured the samples with a commercial Horiba Scientific time correlated single photon counting (TCSPC) system (see Figure 4B–D). The PL lifetime measured by the TCSPC system agreed well with that of our homemade system. It should be noted that the perovskite photodetectors applied here needed neither cooling nor power to operate, and their cost was much lower than existing commercial ones.

The observation of ultrafast extraction of photogenerated carriers in perovskite photodetectors also provides important insight in understanding high-efficiency solar-cell devices because they do have almost the same structure.[33,34,37] This result also answers another puzzle as to whether a bulk heterojunction can form in perovskite solar cells by infiltration of fullerenes into the grain boundaries.[46] The significantly large mobility and quick extraction of charges made this scenario impossible because the charge carriers preferred to transport through the perovskite layer, which represents a highway for carrier transport. The fullerenes in the grain boundaries only fulfilled the function of trap passivation instead of carrier transport, though the fullerene thin layer close to the cathode electrode eventually accepted electrons and transported them to the cathode.

In summary, we have presented a solution-processed OIHP photodetector with an ultrafast response time of ≈1 ns with operation at zero bias. We have demonstrated the application of these low-cost photodetectors by setting up of a TRPL system and successfully measuring a variety of different optoelectronic materials with a radiative recombination lifetime in the range of several nanoseconds to microseconds. To the best of our knowledge, this is the first time a low-cost solution-processed photodetector has been shown to meet the requirements for application in very-high-performance scientific equipment. In addition, we believe these fast photodetectors will find applications in consumer electronics, due to their optimal absorption spectrum for visible imaging, fast response speed for quick frame rate imagers, and array formation by established printing technologies.

Experimental Section

Device Fabrication: PTAA dissolved in toluene was spun on clean ITO substrates at a speed of 5000rpm. The film was then annealed at 100 °C for 10 min. Lead iodine (PbI_2) and methylammonium iodide (MAI) were dissolved in dimethylformamide and 2-propanol with concentrations of 630 and 65 mg mL^{-1}, respectively. The PbI_2 solution was spun on a PTAA layer at 6000 rpm for 35 s. Then the PbI_2 film was transferred onto a hot plate at 90 °C for quick drying. Afterward, the MAI solution was spun on top of the PbI_2 film at 6000 rpm for 35 s at room temperature, combined with a thermal annealing at 100 °C for 1 h. Finally, the device was completed by thermally evaporating C_{60} (30 nm), BCP (8 nm), and Cu (80 nm) in sequential order.

Device Characterization: Air mass 1.5 G simulated irradiation with an intensity of 100 mW cm^{-2} was produced by a xenon-lamp-based solar simulator (Oriel 67005, 150 W) for current (*I*)–voltage (*V*) measurements. The light intensity was calibrated using a silicon diode (Hamamatsu S1133). A Keithley 2400 Source Meter was employed for *I–V* measurements. The voltage scanning rate was 0.1 V s^{-1}. A Keithley 4200 source meter was used to add pulse bias to the device. The thermal admittance spectroscopy and capacitance–voltage characteristic were performed by an Agilent E4980A Precision LCR Meter. The demarcation energy is the cut-off energy that only the trap states below the demarcation energy can capture or emit charges with the given angular frequency and contribute to the capacitance. The temperature dependence of the response speed was measured by the Linkam Scientific Instruments LNP95 cooling system. The OIHP photodetectors was sealed in a cooling stage, and the temperature was precisely controlled by a liquid nitrogen flow with a cooling/heating rate of 5 °C min^{-1}. Each temperature point was held for 30 min before the response speed was recorded. All of the cables that connected the device and oscilloscope needed to be as short as possible and were connected with a fast (6 GHz) bayonet Neill–Concelman connector to minimize the influence of the inductance of the circuit. The oscilloscope was triggered on by the laser signal to record the TPC curve.

Supporting Information

Supporting Information is available from the Wiley Online Library or from the author.

Acknowledgements

This work was supported by the Department of Homeland Security under Award No. 2014-DN-077-ARI069-02, the National Science Foundation under Award No. ECCS-1348272, and the Office of Naval Research under Award No. N000141210556. Huang and Lu also thank the Nebraska Center for Energy Sciences Research for its financial support.

Received: July 7, 2016
Revised: September 7, 2016
Published online: October 26, 2016

[1] X. Wang, W. Tian, M. Liao, Y. Bando, D. Golberg, *Chem. Soc. Rev.* **2014**, *43*, 1400.

[2] F. H. L. Koppens, T. Mueller, P. Avouris, A. C. Ferrari, M. S. Vitiello, M. Polini, *Nat. Nanotechnol.* **2014**, *9*, 780.

[3] Z. Huang, J. E. Carey, M. Liu, X. Guo, E. Mazur, J. C. Campbell, *Appl. Phys. Lett.* **2006**, *89*, 033506.
[4] J. B. D. Soole, H. Schumacher, *IEEE J. Quantum Electron.* **1991**, *27*, 737.
[5] J. Li, Y. Xu, T. Y. Hsiang, W. R. Donaldson, *Appl. Phys. Lett.* **2004**, *84*, 2091.
[6] K. K. Manga, J. Wang, M. Lin, J. Zhang, M. Nesladek, V. Nalla, W. Ji, K. P. Loh, *Adv. Mater.* **2012**, *24*, 1697.
[7] S. A. McDonald, G. Konstantatos, S. Zhang, P. W. Cyr, E. J. D. Klem, L. Levina, E. H. Sargent, *Nat. Mater.* **2005**, *4*, 138.
[8] T. Aernouts, T. Aleksandrov, C. Girotto, J. Genoe, J. Poortmans, *Appl. Phys. Lett.* **2008**, *92*, 033306.
[9] Q. Hu, H. Wu, J. Sun, D. Yan, Y. Gao, J. Yang, *Nanoscale* **2016**, *8*, 5350.
[10] P. Hu, L. Wang, M. Yoon, J. Zhang, W. Feng, X. Wang, Z. Wen, J. C. Idrobo, Y. Miyamoto, D. B. Geohegan, K. Xiao, *Nano Lett.* **2013**, *13*, 1649.
[11] X. Gong, M. Tong, Y. Xia, W. Cai, J. S. Moon, Y. Cao, G. Yu, C. Shieh, B. Nilsson, A. J. Heeger, *Science.* **2009**, *325*, 1665.
[12] L. Zhang, T. Yang, L. Shen, Y. Fang, L. Dang, N. Zhou, X. Guo, Z. Hong, Y. Yang, H. Wu, J. Huang, Y. Liang, *Adv. Mater.* **2015**, *27*, 6496.
[13] Y. Fang, F. Guo, Z. Xiao, J. Huang, *Adv. Opt. Mater.* **2014**, *2*, 348.
[14] F. Guo, B. Yang, Y. Yuan, Z. Xiao, Q. Dong, Y. Bi, J. Huang, *Nat. Nanotechnol.* **2012**, *7*, 798.
[15] H. Wei, Y. Fang, Y. Yuan, L. Shen, J. Huang, *Adv. Mater.* **2015**, *27*, 4975.
[16] V. Coropceanu, J. Cornil, D. A. d. S. Filho, Y. Olivier, R. Silbey, J. Brédas, *Chem. Rev.* **2007**, *107*, 926.
[17] X. Zhou, D. Yang, D. Ma, *Adv. Opt. Mater.* **2015**, *3*, 1570.
[18] D. Zhitomirsky, O. Voznyy, L. Levina, S. Hoogland, K. W. Kemp, A. H. Ip, S. M. Thon, E. H. Sargent, *Nat. Commun.* **2014**, *5*, 3803.
[19] H. Chen, M. K. F. Lo, G. Yang, H. G. Monbouquette, Y. Yang, *Nat. Nanotechnol.* **2008**, *3*, 543.
[20] L. Shen, Y. Fang, H. Wei, Y. Yuan, J. Huang, *Adv. Mater.* **2016**, *28*, 2043.
[21] H. Zhou, Q. Chen, G. Li, S. Luo, T. Song, H. Duan, Z. Hong, J. You, Y. Liu, Y. Yang, *Science* **2014**, *345*, 542.
[22] W. S. Yang, J. H. Noh, N. J. Jeon, Y. C. Kim, S. Ryu, J. Seo, S. I. Seok, *Science* **2015**, *348*, 1234.
[23] D. Bi, W. Tress, M. I. Dar, P. Gao, J. Luo, C. Renevier, K. Schenk, A. Abate, F. Giordano, J. C. Baena, J. Decoppet, S. M. Zakeeruddin, M. K. Nazeeruddin, M. Grätzel, A. Hagfeldt, *Sci. Adv.* **2016**, *2*, e1501170.
[24] Z. Tan, R. S. Moghaddam, M. L. Lai, P. Docampo, R. Higler, F. Deschler, M. Price, A. Sadhanala, L. M. Pazos, D. Credgington, F. Hanusch, T. Bein, H. J. Snaith, R. H. Friend, *Nat. Nanotechnol.* **2014**, *9*, 687.
[25] G. Xing, N. Mathews, S. S. Lim, N. Yantara, X. Liu, D. Sabba, M. Grätzel, S. Mhaisalkar, T. C. Sum, *Nat. Mater.* **2014**, *13*, 476.
[26] H. Zhu, Y. Fu, F. Meng, X. Wu, Z. Gong, Q. Ding, M. V. Gustafsson, M. T. Trinh, S. Jin, X. Zhu, *Nat. Mater.* **2015**, *14*, 636.
[27] L. Dou, Y. M. Yang, J. You, Z. Hong, W. Chang, G. Li, Y. Yang, *Nat. Commun.* **2014**, *5*, 5404.
[28] S. Yakunin, M. Sytnyk, D. Kriegner, S. Shrestha, M. Richter, G. J. Matt, H. Azimi, C. J. Brabec, J. Stangl, M. V. Kovalenko, W. Heiss, *Nat. Photonics* **2015**, *9*, 444.
[29] R. Dong, Y. Fang, J. Chae, J. Dai, Z. Xiao, Q. Dong, Y. Yuan, A. Centrone, X. C. Zeng, J. Huang, *Adv. Mater.* **2015**, *27*, 1912.
[30] Q. Lin, A. Armin, D. M. Lyons, P. L. Burn, P. Meredith, *Adv. Mater.* **2015**, *27*, 2060.
[31] Y. Fang, J. Huang, *Adv. Mater.* **2015**, *27*, 2804.
[32] A. D. d. Z. Mendaza, A. Melianas, S. Rossbauer, O. Bäcke, L. Nordstierna, P. Erhart, E. Olsson, T. D. Anthopoulos, O. Inganäs, C. Müller, *Adv. Mater.* **2015**, *27*, 7325.
[33] C. Bi, Q. Wang, Y. Shao, Y. Yuan, Z. Xiao, J. Huang, *Nat. Commun.* **2015**, *6*, 7747.
[34] Q. Wang, Y. Shao, Q. Dong, Z. Xiao, Y. Yuan, J. Huang, *Energy Environ. Sci.* **2014**, *7*, 2359.
[35] A. Armin, M. Hambsch, I. K. Kim, P. L. Bum, P. Meredith, E. B Namdas, *Laser Photonics Rev.* **2014**, *8*, 924.
[36] B. R. Sutherland, A. K. Johnston, A. H. Ip, J. Xu, V. Adinolfi, P. Kanjanaboos, E. H. Sargent, *ACS Photonics* **2015**, *2*, 1117.
[37] Y. Shao, Z. Xiao, C. Bi, Y. Yuan, J. Huang, *Nat. Commun.* **2014**, *5*, 5784.
[38] R. L. Milot, G. E. Eperon, H. J. Snaith, M. B. Johnston, L. M. Herz, *Adv. Funct. Mater.* **2015**, *25*, 6218.
[39] I. I. Fishchuck, A. K. Kadashchuck, J. Genoe, M. Ullah, H. Sitter, T. B. Singh, H. Bässler, *Phys. Rev. B* **2010**, *81*, 045202.
[40] S. V. Averine, R. Sachot, *IEEE Proc. Optoelectron.* **2000**, *147*, 145.
[41] Q. Wang, Y. Shao, H. Xie, L. Lyu, X. Liu, Y. Gao, J. Huang, *Appl. Phys. Lett.* **2014**, *105*, 163508.
[42] W. K. Bae, Y. Park, J. Lim, D. Lee, L. A. Padilha, H. McDaniel, I. Robel, C. Lee, J. M. Pietryga, V. I. Klimov, *Nat. Commun.* **2013**, *4*, 2661.
[43] S. Cueff, D. Li, Y. Zhou, F. J. Wong, J. A. Kurvits, S. Ramanathan, R. Zia, *Nat. Commun.* **2015**, *6*, 8636.
[44] H. Fang, F. Wang, S. Adjolatse, N. Zhao, J. Even, M. A. Loi, *Light Sci. App.* **2016**, *5*, e16056.
[45] W. K. Metzger, D. Albin, D. Levi, P. Sheldon, X. Li, B. M. Keyes, R. K. Ahrenkiel, *J. Appl. Phys.* **2003**, *94*, 3549.
[46] C. Chiang, C. Wu, *Nat. Photonics* **2016**, *10*, 196.